VERTICALLY AND DENSELY ALIGNED REDUCED GRAPHENE OXIDE/POLYDIMETHYLSILOXANE COMPOSITE FABRICATED BY A TWO-STAGE REDUCTION METHOD FOR HEAT-TRANSFER IN THERMAL INTERFACE MATERIALS

Dong Han[1], Yun-Hong Zhao[1] and Shu-Lin Bai[1]

[1]Department of Materials Science and Engineering, HEDPS/CAPT/LTCS, Key Laboratory of Polymer Chemistry and Physics of Ministry of Education, College of Engineering, Peking University, Beijing 100871, China
Email: wynter001@pku.edu.cn
Email: zhaoyunhonghope@163.com
Email: slbai@pku.edu.cn, Web Page: http://www.coe.pku.edu.cn/faculty-list/f/Bai-Shulin

Keywords: reduced graphene oxide, vertical alignment, PDMS composite, thermal conductivity, thermal interfacial materials

Abstract
Graphene-based thermal conductive composites have been extensively studied in recent years. A considerable amount of works devoted to increase thermal conductivity by increasing the graphene loading of composites. However, it is not practical in the fabrication process when the graphene content is too high. In this work, a novel fabrication method of graphene-based composite is proposed, by which thermal-reduced vertically aligned reduced graphene oxide (TR-VArGO)/polydimethylsiloxane (PDMS) composite was obtained. This method involves mainly two-step reduction of graphene oxide and hand-rolling process of reduced graphene oxide film. Due to the vertical alignment of TR-VArGO film, which provides a rapid and effective heat-transfer pathway, the composite has a high thermal conductivity of 1.349 W m^{-1} K^{-1}, i.e. has an enhancement of as high as 571% compared to pure PDMS, as well as remarkable themostability.

1. Introduction

With the rapid development of modern electronic devices packed with highly integrated circuits, their increasing power densities have caused higher operating temperature, resulting in a major bottleneck of heat dissipation in various devices [1-4]. Great effort has been made for the development of gap-filling thermal interface materials (TIMs) based on carbon materials (e.g., graphite nanoplatelets, carbon nanotubes and carbon fibers) in order to break the bottleneck [4-7].

Graphene, a surprising form of carbon that consists of only one plain layer of atoms arranged in a hexagonal lattice, has extraordinarily high electron mobility [8], mechanical strength [9] and thermal conductivity [10]. Due to these unique properties, graphene has been widely applied in microelectronic devices [11], transparent & flexible electrically conductive films [12] and micro-supercapacitor for energy storage [13], etc. It is noteworthy that a considerable amount of researchers devoted to improve a certain property of graphene-based polymeric composites by increasing the loading of graphene. In contrast, sometimes graphene must be stacked in a 3-D porous structure in electrodes of electrical storage devices to promote rapid ion migration and make full use of its large specific surface area [14]. Therefore, particular arrangements of graphene in various devices are necessary for their diverse

Excerpt from ISBN 978-3-00-053387-7

functions. For TIM application, high thermal conductivity in the out-plane direction is desired [15], so that graphene is expected to be vertically stacked between contact solid interfaces.

Yoon et al. [16] reported a method to fabricate vertically aligned reduced graphene oxide (VArGO). First, GO film was obtained by spontaneous evaporation overnight. Then the films were rolled to get vertically aligned architecture. Finally, VArGO film was formed by thermal annealing at the temperature up to 1000 ℃ for 1 h. Herein, we report a more efficient method to fabricate thermal-reduced VArGO (TR-VArGO)/polydimethylsiloxane (PDMS) composite, which has a high thermal conductivity of 1.349 W m^{-1} K^{-1}, i.e. an enhancement of as high as 571% compared to pure PDMS.

2. Experimental

2.1. Fabrication of reduced graphene oxide (rGO) film

Well-dispersed GO dispersion (6 mg mL^{-1}) was prepared from natural graphite powder (Sinopharm Chemical Reagent Co., Ltd) based on a modified Hummers method [13]. The dispersion was then diluted to 3 mg mL^{-1} with predetermined HCl aqueous solution (10^{-3} mol L^{-1}) and sonicated for 3 h. The Zn foil (Benchely) was immersed into the acidified GO dispersion for interfacial gelation for 3 h. Then interfacial gel grown on Zn surface was thoroughly washed with deionized water so as to remove physically adsorbed GO sheets. Immediately following the washing step, the gel film was detached from Zn foil by 20 fold diluted HCl etching and transferred into aqueous HCl solution for another 5 h to dissolve residual Zn impurities. Finally, the as-prepared rGO gel film was kept in deionized water.

2.2. Fabrication of vertically aligned rGO/polyvinyl alcohol (VArGO/PVA) composite

Firstly, the rGO gel film was transferred from deionized water into 4 wt.% aqueous solution of PVA (PVA-124, Sinopharm Chemical Reagent Co., Ltd, average molecular weight 105000 g mol^{-1}). Then the rGO film was moved on a piece of polyethylene glycol terephthalate (PET) membrane, hung up to remove redundant aqueous PVA solution, and dried at room temperature for 5 h. After thoroughly drying, it was easy to peel off the rGO/PVA composite film from the PET membrane, and the composite film was of sufficient strength to proceed the rolling-up process.Then the as-fabricated rGO/PVA composite film was cut into narrow strips (3 mm in width) and were manually rolled up to get a VArGO/PVA composite disc sample with a diameter of 12.7 mm and thickness of 3 mm.

2.3. Fabrication of thermal-reduced VArGO (TR-VArGO)

TR-VArGO was formed by thermal reduction treatment which included a three-stage temperature-rise period and a 30 min-holding stage. The thermal reduction process is as follows: firstly, the samples were put in a U-type quartz tube installed in a temperature programmable furnace (SGL-1200, Shanghai Daheng), then were heated from room temperature to 200 ℃ at the rate of 0.5 ℃/min under an argon flow (100 s.c.c.m.); secondly, the temperature was increased from 200 to 400 ℃ at a slower ramp rate of 0.2 ℃/min; thirdly, the samples were heated up to 1000 ℃ at the rate of 2 ℃/min, and then the specific temperature was kept for 30 min under the same argon flow; finally, the furnace cooling was followed until room temperature to get pure TR-VArGO samples.

2.4. Fabrication of TR-VArGO/PDMS composites

TR-VArGO/PDMS composites were prepared in suitable molds by infiltrating the TR-VArGO with liquid PDMS prepolymer and a viscous mixture of base and curing agent (Sylgard 184, Dow Corning, base/curing agent = 10/1 in weight), followed by vacuum outgassing in a vacuum oven for 20 min and then thermally curing at 80 ℃ for 4 h to obtain the composite sample. The top and bottom surfaces of

Excerpt from ISBN 978-3-00-053387-7

as-prepared TR-VArGO/PDMS composite disc were slicked by slight and careful cutting and a final dimension of samples is 12.7 mm (diameter) × 2 mm (thickness).

2.5. Characterization of materials

The morphological and microstructural characterizations of as-obtained samples were performed using a scanning electron microscope (SEM, S-4800, HITACHI) operated at 10 kV. Laser Raman spectroscopy was performed using HORIBA Jobin Yvon LabRAM HR Evolution Raman spectrometer with He-Ne laser excited at 514.5nm with the power of 150 uw/cm^2. All X-ray photoelectron spectroscopy (XPS) measurements were conducted by Axis Ultra imaging photoelectron spectrometer (Kratos Analytical Ltd.) with a monochromatic Al Kα X-ray source at 225 W. Values of thermal conductivity were calculated from the equation $k = \alpha\rho C_p$, where k, α, ρ and C_p represent thermal conductivity, thermal diffusivity, material bulk density and specific heat capacity, respectively. Thermal diffusivity was measured by a laser flash apparatus (LFA 447 Nanoflash, NETSZCH). Bulk density was calculated from sample weight and volume. Specific heat capacity was obtained by a differential scanning calorimeter (DSC, Q2000, TA). Dynamic thermogravimetric analysis was performed on a thermogravimetric Analyzer (Q600 SDT, TA).

3. Results and discussion

Generally, rGO film is formed by one-step thermal reduction of paper-like aligned GO film which is prepared by a vacuum assisted flow-filtration method [17, 18]. In order to increase the efficiency in the film-forming process, we transformed the reduction procedure into a two-stage process (Figure 1). Firstly, according to a interfacial-gel method reported by Maiti et al. [19], we prepared metal-reduced rGO (MR-rGO) film instead of GO film on zinc foil template. Meanwhile, to make sure that the as-prepared rGO film has sufficient strength to proceed the rolling-up process, it was immersed into 4 wt.% aqueous solution of PVA, and after thoroughly dried, rGO/PVA composite film was formed. The composite film with sufficient tensile strength can be cut into strips and rolled into VArGO/PVA composite. In the following thermal reduction process, TR-VArGO was formed by a three-stage temperature-rise period and a 30 min-holding stage. Finally, TR-VArGO/PDMS composite was fabricated in suitable molds by infiltrating the as-made TR-VArGO with PDMS prepolymer.

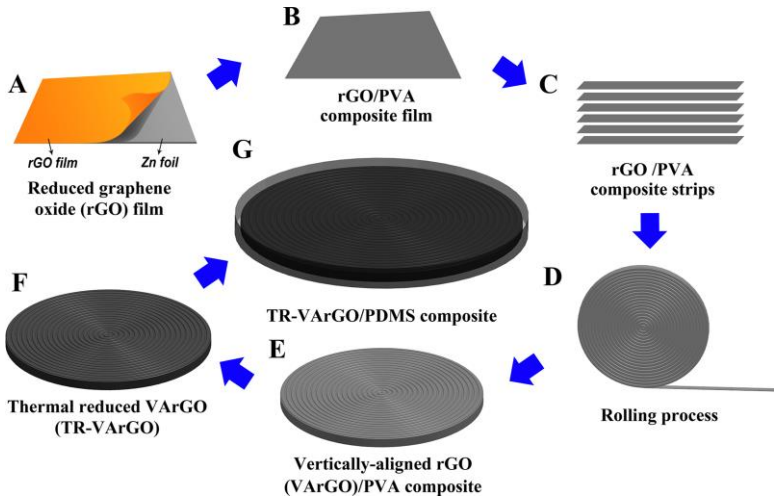

Figure 1. Schematic fabrication procedure of thermal-reduced vertically aligned reduced graphene oxide (TR-VArGO)/PDMS composite.

Excerpt from ISBN 978-3-00-053387-7

3.1. Morphologies and microstructures of VArGO/PVA composite and TR-VArGO

The morphologies and microstructures of the VArGO/PVA composite and TR-VArGO samples are shown in Figure 2. It is clearly seen that the VArGO/PVA composite is densely piled after simple hand rolling process and vertically aligned films are stuck tightly together due to the addition of PVA. The arrows in Figure 2a point out some extended PVA filaments bridging a small amount of gaps between layers. Nevertheless, the gaps between layers can benefit the penetration of liquid polymer in the following fabrication of composite. Because PVA can be completely decomposed at about 600 ℃ [18], thus further thermal reduction of VArGO/PVA composite via a staged heating process up to 1000 ℃ removed all the PVA adhered on the surface of VArGO, and then pure TR-VArGO samples were obtained. As seen in Figure 2b, TR-VArGO without PVA shows similar morphology with VArGO/PVA composite. From insets in Figure 2, it can also be confirmed that there is almost no differences between these two samples, the vertically aligned architecture of VArGO was retained after high temperature thermal reduction.

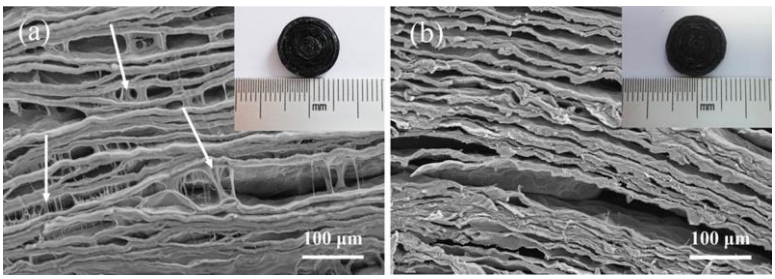

Figure 2. SEM images of top surfaces of (a) VArGO/PVA composite and (b) TR-VArGO. Insets showing the digital camera images of samples.

3.2. Chemical composition and structure characterizations

Two-stage reduction of GO removed most oxygen functional groups of itself to give highly reduced rGOs [17-19]. The oxygen content of GO illustrated in Table 1, is as high as 54.69 at.% and that of rGO was reduced gradually with the progress of reduction. XPS was used to quantitatively analyze the element content (Table 1) and chemical structure of GO, MR-rGO and TR-rGO. The deconvoluted XPS C1s spectra of these samples (Figure 3a) show three peaks for graphitic structure (C-C/C=C at 284.8 eV), hydroxyl/epoxy groups (C-O at 286.8 eV), and carbonyl group (O-C=O at 288.5 eV), respectively. The C-O bands come from epoxy and hydroxyl groups in the basal plane [19]. The C=O compounds mainly arose from single ketones [20] which decorates the edges of GO sheets but may also be bound to the basal plane as carbonyl groups [21]. Compared to the XPS C1s spectrum of GO (Figure 3a), sharp decrease of the peak intensities for oxygen functional groups in the XPS C1s spectra of MR-rGO and TR-rGO indicates a high level reduction degree of GO after two-stage treatment. Moreover, the evolution of carbon bonds is also quantitated as shown in Table 2. It is obvious that the carbon sp^2 fraction increased with the progress of reduction, while the content of oxygen-containing functionalities (C-O and C=O) decreased.

Table 1. Summary of the elemental compositions of materials.

Sample	C^a (%)	O^a (%)	$I_D/I_G{}^b$
GO	45.31	54.69	0.92
MR-rGO	82.04	17.96	1.89
TR-rGO	92.94	7.06	1.29

Excerpt from ISBN 978-3-00-053387-7

[a] Determined by low-resolution scanning XPS spectra.
[b] Determined by Raman.

Table 2. Fitted binding energy (B.E.) and atomic ratio (at. %) of the C1s XPS spectra of samples

B.E. (eV)	C1 (284.8)	C2 (286.8)	C3 (288.5)
Assignment	C-C/C=C	C-O	O-C=O
GO	39.01	54.51	6.48
MR-rGO	64.49	28.48	7.03
TR-rGO	80.77	13.24	5.99

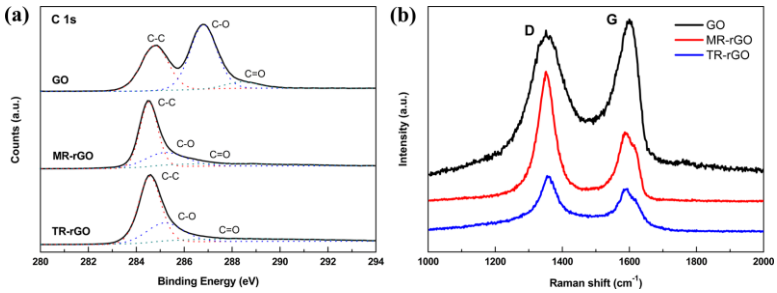

Figure 3. (a) XPS C1s spectra, (b) Raman spectra of GO, MR-rGO and TR-rGO.

Raman was performed to further investigate the texture of the samples. The Raman spectra of GO, MR-rGO and TR-rGO (Figure 3b) show two characteristic peaks at ~1352 cm^{-1} and ~1594 cm^{-1}, corresponding to D and G bands of graphene, respectively. As shown in Table 1, the ratio of I_D/I_G rises from 0.92 of GO to 1.89 of MR-rGO after the metal reduction, owing to an increase in structural defects which is attributable to the desorption of oxygen bonded saturated sp^3 carbons as CO_2 and/or CO (especially from epoxy groups) [22]. It is of vital importance to remove the oxygen contained in the GO during the reduction process, as sp^2 clusters in GO are isolated by oxygen atoms and a reduction by removal of O results in greater connectivity among the existing graphitic domains by the formation of new sp^2 domains [22, 23]. Surprisingly, a significant decrease in the I_D/I_G ratio from 1.89 to 1.29 is observed after thermal annealing treatment, which is ascribed to the recovery of sp^2-hybridized carbon-carbon bonds of the graphitic lattice and connection of new sp^2 clusters in the samples through thermal treatment [24].

3.3. Morphology and microstructure of TR-VArGO/PDMS composite

Figure 4 shows the morphologies of top surface and longitudinal section of TR-VArGO/PDMS composite (the filler loading is 15.65 wt.%). It can be clearly seen in Figure 4a and inset that the arc-shaped rGO layers are embedded in PDMS matrix, i.e. the gaps between rGO layers (Figure 2b) are filled with PDMS, making TR-VArGO and PDMS be combined into a uniform bulk material. Expectantly, there exist few of small crevices between rGO layers and PDMS matrix, indicating a good interface-bonding between filler and matrix. It can also be observed in Figure 4b that the longitudinal section of cryo-fractured surface is homogeneous.

Excerpt from ISBN 978-3-00-053387-7

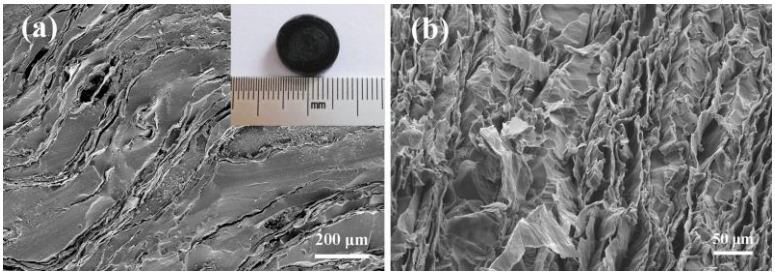

Figure 4. SEM images of (a) Top surface and (b) Longitudinal section of TR-VArGO/PDMS composite. Inset showing the digital camera image of sample.

3.4. Thermal Properties

Thermal diffusivity of TR-VArGO/PDMS composite and pure PDMS was measured by a laser flash apparatus. Quantitative values of thermal diffusivity are given in Table 3. Furthermore, specific heat capacity was measured by a differential scanning calorimeter and bulk density was calculated from sample weight and volume (Table 3).

Table 3. A summary of detailed sample information and thermal properties

Sample	α (mm^2/s)	ρ (g/cm^3)	Cp ($J\ g^{-1}\ K^{-1}$)	k ($W\ m^{-1}\ K^{-1}$)	Mass fraction (wt.%)
PDMS	0.128	0.988	1.592	0.201	-
TR-VArGO/PDMS	1.069	0.895	1.410	1.349	15.65

As detailed in Table 3, the values of thermal conductivity and thermal diffusivity of as-prepared 15.65 wt.% TR-VArGO/PDMS composite are 1.349 $W\ m^{-1}\ K^{-1}$ and 1.069 mm^2/s (measured at 25 ℃), i.e. 6.71 and 8.35 times that of pure PDMS, respectively. It is noticed in Table 3 that thermal conductivity of TR-VArGO/PDMS composite is mainly determined by the thermal diffusivity, which measures the ability of a material to conduct thermal energy relative to its ability to store thermal energy. Furthermore, it is well-known that TR-rGO has much higher thermal diffusivity than PDMS, so the high thermal conductivity of composite is primarily contributed by TR-VArGO.

As is well-known, TIMs are applied between heat sources and heat sinks. The operating temperature rises continually with rapidly increasing power densities in electronic devices. Therefore, better TIMs should have not only high thermal conductivity, but also good thermostability. As shown in Figure 5, the mass loss of the samples was divided into three stages as follow: (I) from 30 to 250 ℃, the physically absorbed water on the surface of the samples was evaporated [25]; (II) from 250 to 600 ℃, the degradation rate became very quick, and almost all polymer chains were degraded abruptly within this temperature range. Such a high weight loss comes from the fierce decomposition of oxygen-containing functional groups in the polymer matrix and the released small molecules were determined to be H_2O, CO and CO_2. [25]; (III) from 600 to 900 ℃, residual oxygen-containing functional groups were removed steadily, resulting in almost no weight loss in this stage. The TG curve of TR-VArGO/PDMS composite shows an obviously shift to higher temperature. This reveals that the addition of TR-VArGO can improve the thermal stability of PDMS. According to Lee et al. [26], the weight loss may be related with the breakdown of the main molecular chains which induced polymer decomposition. Filling of TR-VArGO may hinder the diffusion of volatile decomposition products such as H_2O, CO and CO_2 and thus improved the thermostability of polymers [27].

Excerpt from ISBN 978-3-00-053387-7

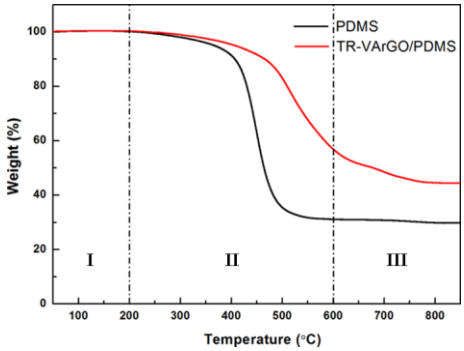

Figure 5. Thermogravimetic analysis of pure PDMS and TR-VArGO/PDMS composite.

4. Conclusions

In summary, a two-stage reduction method and a simple rolling process were proposed to prepare vertically and compactly aligned reduced graphene oxide (VArGO)/PDMS composite. A high reduction level of thermal-reduced VArGO (TR-VArGO) is achieved using the two-stage method. The rolling process guarantees the vertical and compact alignment of TR-VArGO in the composite. The thermal conductivity of TR-VArGO/PDMS composite is up to 1.349 W m^{-1} K^{-1} and the thermal conductivity enhancement is as high as 571%. The use of TR-VArGO film improve the thermostabiliy of the composite. The high performance of TR-VArGO/PDMS composite synthesized by a simple and facile process in this work shows promising potentials in thermal management of microelectronic devices and photonic applications.

Acknowledgments

The authors would like to thank the support by NSFC and NSFC-RGC Joint Research Scheme (Nos. 11272008, 11361161001, 11202005 and CUHK450/13).

References

[1] R. Prasher. Thermal interface materials: historical perspective, status, and future directions. *Proceedings of the IEEE*, 94: 1571–1586, 2015.

[2] A. A. Balandin. Thermal properties of graphene and nanostructured carbon materials. *Nature Materials*, 10: 569–581, 2011.

[3] A.J. McNamara, Y. Joshi, Z.M. Zhang. Characterization of nanostructured thermal interface materials – a review. *International Journal of Thermal Sciences*, 62: 2–11, 2012.

[4] A. Yu, P. Ramesh, X.B. Sun, E. Bekyarova, M.E. Itkis, and R.C. Haddon. Enhanced thermal conductivity in a hybrid graphite nanoplatelet–carbon nanotube filler for epoxy composites. Advanced Materials, 20: 4740–4744, 2008.

[5] A.Yu, P. Ramesh, M.E. Itkis, E. Bekyarova, and R.C. Haddon. Graphite nanoplatelet-epoxy composite thermal interface materials. *The Journal of Physical Chemistry C*, 111: 7565–7569, 2007.

[6] J. Hong, J. Lee, C.K. Hong, S.E. Shim. Effect of dispersion state of carbon nanotube on the thermal conductivity of poly(dimethyl siloxane) composites. *Current Applied Physics*, 10: 359–363, 2010.

[7] Y.M. Chen, J.M. Ting. Ultra high thermal conductivity polymer composites. *Carbon*, 40: 359–362, 2002.

Excerpt from ISBN 978-3-00-053387-7

[8] K.I. Bolotin, K.J. Sikes, Z. Jiang, M. Klima, G. Fudenberg, J. Hone, P. Kim, and H.L. Stormer. Ultrahigh electron mobility in suspended graphene. *Solid State Communications*, 146: 351–355, 2008.

[9] C. Lee, X. Wei, J.W. Kysar, J. Hone. Measurement of the elastic properties and intrinsic strength of monolayer graphene. *Science*, 321: 385–388, 2008.

[10] A.A. Balandin, S. Ghosh, W. Bao, I. Calizo, D. Teweldebrhan, F. Miao, and C.N. Lau. Superior thermal conductivity of single-layer graphene. *Nano Letters*, 8: 902–907, 2008.

[11] M.C. Lemme, T.J. Echtermeyer, M. Baus, and H. Kurz. A graphene field-effect device. *IEEE Electron Device Letters*, 28: 282–284, 2007.

[12] G. Eda, G. Fanchini, M. Ghhowalla. Large-area ultrathin films of reduced graphene oxide as a transparent and flexible electronic material. *Nature Nanotechnology*, 3: 270–274, 2008.

[13] Z.K. Wu, Z. Lin, L. Li, S.L. Bai, C.P. Wong. Flexible micro-supercapacitor based on in-situ assembled graphene on metal template at room temperature. *Nano Energy*, 10: 222–228, 2014.

[14] M.D. Stoller, S. Park, Y. Zhu, J. An, and R.S. Ruoff. Graphene-based ultracapacitors. *Nano Letters*, 8: 2498–3502, 2008.

[15] J. Xu, T.S. Fisher. Enhancement of thermal interface materials with carbon nanotube arrays. *International Journal of Heat and Mass Transfer*, 49: 1658–1666, 2006.

[16] Y. Yoon, K. Lee, S. Kwon, S. Seo, H. Yoo, S. Kim, Y. Shin, Y. Park, D. Kim, J.Y. Choi, H. Lee. Vertical alignments of graphene sheets spatially and densely piled for fast ion diffusion in compact supercapacitors. *ACS Nano*, 8: 4580–4590, 2014.

[17] N.J. Song, C.M. Chen, C. Lu, Z. Liu, Q.Q. Kong, and R. Cai. Thermally reduced graphene oxide films as flexible lateral heat spreaders. *Journal of Materials Chemistry A*, 2: 16563–16568, 2014.

[18] Q.Q. Kong, Z. Liu, J.G. Gao, C.M. Chen, Q. Zhang, G. Zhou, Z.C. Tao, X.H. Zhang, M.Z. Wang, F. Li, and R. Cai. Hierarchical graphene–carbon fiber composite paper as a flexible lateral heat spreader. *Advanced Functional Materials*, 24: 4222–4228, 2014.

[19] U.N. Maiti, J. Lim, K.E. Lee, W.J. Lee, and S.O. Kim. Three-dimensional shape engineered, interfacial gelation of reduced graphene oxide for high rate, large capacity supercapacitors. *Advanced Materials*, 26: 615–619, 2013.

[20] G. Xie, Z. Wang, Z. Cui, Y. Shi. Ni–Fe–Co–P coatings on coiled carbon nanofibers. *Carbon*, 43: 3181–3183, 2005.

[21] W. Cai, R.D. Piner, F.J. Stadermann, S. Park, M.A. Shaibat, Y. Ishii, D. Yang, A. Velamakanni, S.J. An, M. Stoller, J. An, D. Chen, R.S. Ruoff. Synthesis and solid-state NMR structural characterization of 13C-labeled graphite oxide. *Science*, 321: 1815–1817, 2008.

[22] C. Mattevi, G. Eda, S. Agnoli, S. Miller, K.A. Mkhoyan, O. Celik, and M. Chhowalla. Evolution of electrical, chemical, and structural properties of transparent and conducting chemically derived graphene thin films. *Advanced Functional Materials*, 19: 2577–2583, 2009.

[23] H. Wang, J.T. Robinson, X. Li, and H. Dai. Solvothermal reduction of chemically exfoliated graphene sheets. *Journal of the American Chemical Society*, 131: 9910–9911, 2009.

[24] C. Vallés, J.D. Núñez, A.M. Benito, and W.K. Maser. Flexible conductive graphene paper obtained by direct and gentle annealing of graphene oxide paper. *Carbon*, 50: 835–844, 2012.

[25] C.M. Chen, J.Q. Huang, Q. Zhang, W.Z. Gong, Q.H. Yang, M.Z. Wang. Annealing a graphene oxide film to produce a free standing high conductive graphene film. *Carbon*, 50: 659–667, 2012.

[26] J.Y. Lee, Y. Liao, R. Nagahata, S. Horiuchi. Effect of metal nanoparticles on thermal stabilization of polymer/metal nanocomposites prepared by a one-step dry process. *Polymer*, 47: 7970–7979, 2006.

[27] H. Qin, S. Zhang, C. Zhao, M. Feng, M. Yang, Z. Shu, S. Yang. Thermal stability and flammability of polypropylene/montmorillonite composites. *Polymer Degradation and Stability*, 85: 807–813, 2004.

Excerpt from ISBN 978-3-00-053387-7